Journal of Power Sources 222 (2013) 38–44

Contents lists available at SciVerse ScienceDirect

Journal of Power Sources

journal homepage: www.elsevier.com/locate/jpowsour

A simple preparation method for quasi-solid-state flexible dye-sensitized solar cells by using sea urchin-like anatase TiO_2 microspheres

Ke Fan, Tianyou Peng*, Junnian Chen, Xiaohu Zhang, Renjie Li

College of Chemistry and Molecular Science, Wuhan University, Wuhan 430072, PR China

HIGHLIGHTS

- Sea urchin-like TiO_2 spheres were used to prepare flexible electrode.
- Quasi-solid state dye-sensitized solar cell was fabricated by the electrode.
- TiO_2 spheres can supply sufficient surface area for dye adsorption.
- Sea urchin-like structures ensure good particle interconnection.
- TiO_2 sphere-based flexible cell shows higher efficiency than the P25-based one

ARTICLE INFO

Article history:
Received 30 March 2012
Received in revised form
15 June 2012
Accepted 22 August 2012
Available online 31 August 2012

Keywords:
TiO_2 microsphere
Dye-sensitized solar cell
Flexible substrate
Low temperature fabrication

ABSTRACT

Sea urchin-like anatase TiO_2 microspheres with hierarchical structure were prepared by a solvothermal method, and were applied for fabricating quasi-solid-state flexible dye-sensitized solar cells through a simple method of mixing it with ethanol and HCl. The flexible solar cells were investigated by the methods of electrochemical impedance spectra, open-circuit voltage decay and photocurrent–voltage curves. It is found that the hierarchical TiO_2 microsphere-based solar cell shows encouraging performance (shot-circuit current density of 11.49 mA cm^{-2}, open-circuit voltage of 0.67 V, fill factor of 0.56, and conversion efficiency of 4.32%), which is much better than that of commercial TiO_2 nanoparticles (P25)-based one, due to its excellent particle interconnections, low electron recombination and high specific surface area.

1. Introduction

Dye-sensitized solar cells (DSSCs) have been widely investigated in recent years due to their low-cost and relatively high conversion efficiency [1]. It was reported that the efficiency of DSSC fabricated on transparent conductive glass had exceeded 12% [2,3]. Generally, DSSCs are mainly composed of three parts: the dye-sensitized nanocrystal film as photoanode, the redox couple (usually I_3^-/I^-) in organic solvent(s), and the platinized transparent conducting oxide (TCO) glass as the counter electrode. Among those, the photoanode usually consists of porous TiO_2 film adsorbed by dye molecules (such as a ruthenium complex), which can absorb the light energy especially the visible light of sunshine. The dye molecules move to the excited states when the DSSC is exposed to light irradiation with suitable energy, and the excited-state electrons are injected quickly into the conduction band of TiO_2; these injected electrons are collected through the conducting substrate of the TiO_2 photoanode. The dye molecules can be regenerated by the iodide ions in the electrolyte, and then the resulting triiodide ions accept electrons from the platinized TCO counter electrode to fulfil a complete current cycle in DSSCs.

Because of the glass substrate's drawbacks such as expensive, rigid and heavy-weight, a branch of DSSCs research has currently focused on the development of inexpensive flexible solar cells fabricated on conductive and light-weight plastic substrates. However, the conventional method for the preparation of glass-based TiO_2 electrodes for DSSCs by using colloidal suspension of TiO_2 nanoparticles requires high temperature sintering at 450–550 °C, which is necessary to establish a good interconnection among the TiO_2 nanoparticles and remove the organic additives. Therefore, a crucial technology in the manufacture of plastic-based DSSCs is low temperature (<150 °C) heat treatments of the photoanode because of the low melting points of the plastic substrates. At such low temperature (<150 °C), the interconnection among

* Corresponding author. Tel./fax: +86 27 6875 2237.
E-mail address: typeng@whu.edu.cn (T. Peng).

0378-7753/$ – see front matter © 2012 Elsevier B.V. All rights reserved.
http://dx.doi.org/10.1016/j.jpowsour.2012.08.054

TiO_2 nanoparticles is usually poor and the residue of organic binder would also increase the resistance of the electrode. Therefore, the performances of most plastic-based DSSCs are lower than those of the conductive glass-based ones. For addressing this issue, to date low temperature preparation methods, such as chemical sintering [4,5], mechanical pressure [6–8], transfer method [9,10], binder-free method [11–14] or adding titanium alkoxides to TiO_2 paste as linking agent [15,16], have been developed to enhance the nanoparticle interconnection in the photoanodes. Although some of the above methods have shown encouraging results, the processes are complicated. Moreover, some one-dimensional TiO_2 nanostructured materials such as nanowires and nanotubes have also been used for the plastic-based DSSCs [17,18], and the poor particle necking resulted from the low temperature preparation method can be addressed due to their one-dimensional structures. However, the specific surface areas of most one-dimensional TiO_2 materials are relatively small, leading to insufficient dye adsorption and poor performances of the solar cells.

Herein, a simple and one-step solvothermal method was used to synthesize sea urchin-like hierarchical anatase TiO_2 microspheres with high specific surface area, which are composed of TiO_2 nanoparticles and hierarchical TiO_2 nanoribbons. Applying these hierarchical TiO_2 microspheres to flexible DSSCs based on conductive plastics *via* a simple method without any binder or sintering process, an encouraging efficiency of 4.32% was obtained. Comparing with commercial TiO_2 nanoparticles (P25), the present hierarchical TiO_2 microspheres display superior performance due to its better particle interconnection, higher dye adsorption and lower charge recombination.

2. Experimental section

2.1. Synthesis of sea urchin-like anatase TiO_2 microspheres

Sea urchin-like anatase TiO_2 microspheres were prepared *via* a modified method described in the previous report [19]. 4 mL of tetrabutoxytitanium (TBOT) was added dropwise to 120 mL of acetic acid under stirring, and then the resultant mixture was transferred to a 200 mL autoclave. After maintaining the autoclave at 140 °C for solvothermal reaction for 72 h, the precursor was obtained by centrifugation and rinsed with water and alcohol, and then calcined at 500 °C for 2 h to get anatase TiO_2 microspheres.

2.2. Flexible TiO_2 photoanode preparation and solar cell assembly

The anatase TiO_2 microspheres (0.2 g) was mixed with 0.6 g ethanol and 0.2 g HCl solution (pH ~ 4.0) by magnetic stirring overnight to make a homogeneous paste. The paste was spread onto the clean conductive indium tin oxide–polyethylene terephthalate (ITO–PET) substrate (~20 Ω/sq.) by doctor-blading technique, and two parallel adhesive tapes (Scotch, approximately 50 μm) were used to control the film thickness and served as spacers. After drying in the air and heat-treating at 150 °C for 1 h, the TiO_2 microspheres film with thickness of ~9 μm was obtained, which was dipped in 0.3 mM N719 dye (Solaronix, Switzerland) ethanol solution overnight. Subsequently, it was washed with anhydrous alcohol and dried at 70 °C. A thin layer of iodine-free quasi-solid-state electrolyte [20] (50 mg 1,2-dimethyl-3-propylimidazolium iodide (DMPII), 0.12 g KI, and 0.40 g polyethylene oxide (PEO),100,000 in 2.5 mL acetonitrile) was cast on the top of TiO_2/dye layer, and then a sputtered Pt on ITO–PET plate as counter electrode was assembled to finish the flexible DSSC. As a comparison, a flexible DSSC fabricated with film electrode of commercial TiO_2 nanoparticles (P25, Deggusa) with average diameter of ~24 nm, which has a thickness similar to the TiO_2 microspheres film, was also fabricated by using the same process.

2.3. Instrumentation and measurements

Structure phase analyses of samples were performed on Bruker D8-advance X-ray diffractometer (XRD) with Cu K_α radiation ($\lambda = 0.15418$ nm). The morphologies of samples were observed by using scanning electron microscope (SEM, JEOL) and transmission electron microscope (TEM, JEOL). To estimate the dye-adsorbed amount on the TiO_2 films, the dye-sensitized electrode was immersed into a 0.1 M NaOH solution in a mixed solvent (water : ethanol = 1:1) at room temperature, which can result in the desorption of N719. The absorbance of the resulting solution was measured by a UV-3600 UV–vis spectrophotometer (Shimadzu, Japan). The dye-adsorbed amount was determined by the molar extinction coefficient of 1.41×10^4 dm^3 mol^{-1} cm^{-1} at 515 nm as reported previously [21].

The electrochemical impedance spectrum (EIS) measurements were carried out by applying open-circuit voltage under illumination, and recorded over a frequency range of 0.05 Hz–100 kHz with ac amplitude of 10 mV. The obtained spectra were fitted with Z-View software (v2.1b, Scribner Associate, Inc.) in term of appropriate equivalent circuit [4]. For the photoinduced open-circuit voltage decay (OCVD) measurements, the solar cell was first illuminated to a steady voltage, and then the illumination was turned off by using a shutter to record the open-circuit photovoltage decay curves. The flexible DSSC was illuminated by light with energy of a 100 mW cm^{-2} from 300 W AM1.5G simulated sunlight (Oriel, USA). The light intensity was determined using a reference monocrystalline silicon cell system (Oriel, USA). A computer-controlled potentiostat (CHI 618) was employed to collect the current–voltage (I–V) curves. The active areas of all the DSSCs are 0.25 cm^2. The photoelectric conversion efficiency was calculated according to the following equation:

$$\eta = \frac{V_{oc} J_{sc} FF}{P_{in}}$$

where η is the global efficiency, V_{oc}, J_{sc}, and FF are open-circuit voltage, short-circuit current density, and fill factor, respectively. P_{in} is the incident light energy (100 mW cm^{-2}).

3. Results and discussion

3.1. Microstructure analyses of sea urchin-like TiO_2 microspheres

Fig. 1a and b show the SEM images of the as-prepared TiO_2 sample derived from solvothermal treatment at 140 °C for 72 h and calcination at 500 °C for 2 h. As can be seen, the TiO_2 sample displays morphology of sea urchin-like microspheres with average diameters of ~3 μm, and the microspheres are composed of TiO_2 nanoparticles and TiO_2 nanoribbons. From the TEM images shown in Fig. 1c and d, the structure of the sea urchin-like TiO_2 microspheres can be observed clearly. It is obvious that the microspheres are composed of nanoparticles and nanoribbons, while the nanoribbons show a hierarchical structure composing of small nanoparticles as shown in the high magnification TEM image (Fig. 1d). Therefore, the whole sea urchin-like TiO_2 displays morphology of hierarchical microsphere with secondary structure. The small nanoparticles with average diameter of ~15 nm in the hierarchical TiO_2 microspheres are much smaller than the commercial TiO_2 nanoparticles (P25) with average diameter of ~24 nm, implying higher specific surface area for more dye-loading to the film electrode.

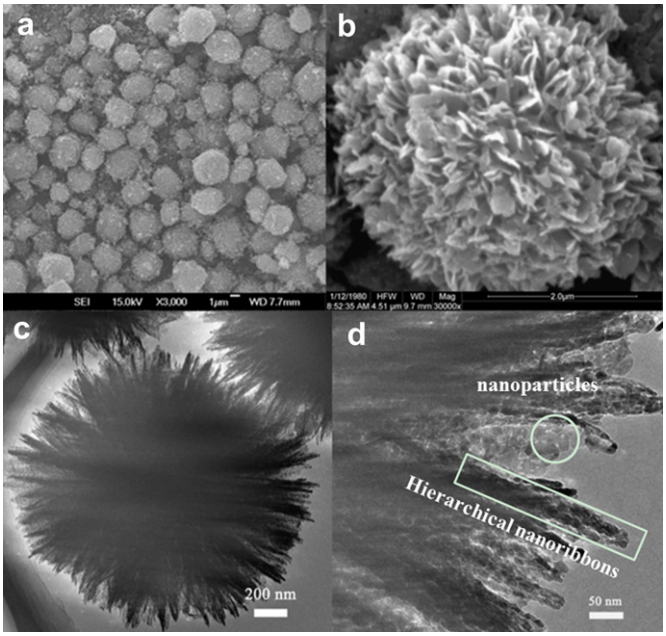

Fig. 1. SEM (a, b) and TEM (c, d) images of the TiO_2 samples derived from solvothermal treatment at 140 °C for 72 h and calcination at 500 °C.

Fig. 2 presents the high resolution transmission electron microscope (HRTEM) image of the sea urchin-like TiO_2 microspheres. The lattice fringes with interplanar distances of 0.352 nm, which are in good agreement with the *d*-spacing values of the anatase (101) planes, can be observed clearly in the HRTEM image. It indicates the high crystallinity of the anatase TiO_2 microspheres. Fig. 3 shows the XRD pattern of the hierarchical TiO_2 microspheres. All the diffraction peaks of the XRD pattern can be indexed to anatase TiO_2, implying the crystal phase of the obtained sea urchin-like TiO_2 microspheres is anatase, which is consistent with the observation from the HRTEM image in Fig. 2. And anatase is more photoactive than the other phases (*e.g.* rutile and brookite) of TiO_2 for DSSCs.

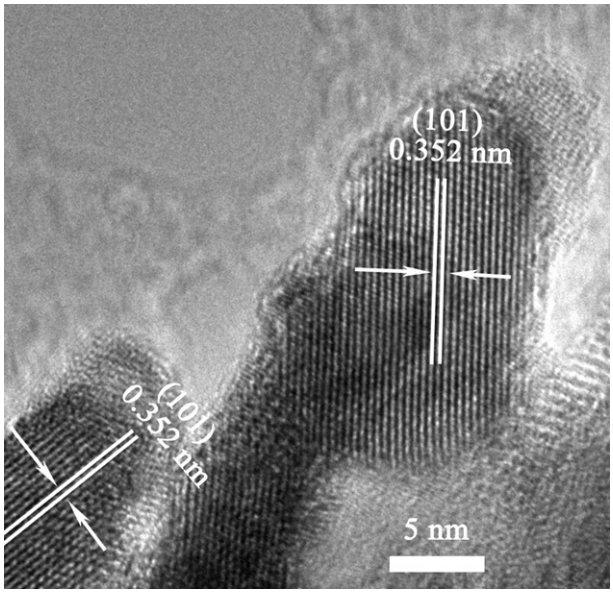

Fig. 2. HRTEM image of the obtained sea urchin-like TiO_2 microspheres.

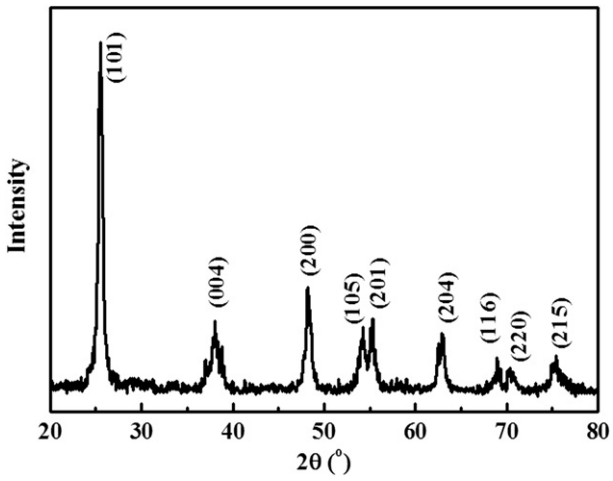

Fig. 3. XRD patterns of the TiO_2 samples derived from solvothermal treatment at 140 °C for 72 h and calcination at 500 °C.

Fig. 4 shows nitrogen adsorption–desorption isotherm and the inset shows Barret–Joyner–Halenda (BJH) pore size distribution plot of the hierarchical TiO_2 microspheres. The isotherm in Fig. 4 displays a typical type IV curve, which is usually attributed to the predominance of mesopores. It reveals the specific surface area of the sea urchin-like TiO_2 microspheres is ~97 $m^2\ g^{-1}$, which is much larger than that (~50 $m^2\ g^{-1}$) of P25. The inset shows the hierarchical TiO_2 microspheres mainly contain mesopores with ~10 nm pore width, which can be attributed to the inner pores of the hierarchical TiO_2 microspheres.

Fig. 5 shows the SEM image and the photograph of the film electrode made of the sea urchin-like TiO_2 microspheres on ITO–PET substrates. As can been seen from Fig. 5a, the film is composed of relatively uniform TiO_2 microspheres, and no any obvious crack can be found. It has been reported that the high adhesion to the hydrophobic surface of the plastic substrate for flexible DSSCs plays a critical role for electron transfer from the TiO_2 film to the substrate. No crack or exfoliation can be found from the photograph (Fig. 5b) of the hierarchical TiO_2 microsphere film on the ITO–PET substrate under bending, indicating the good necking

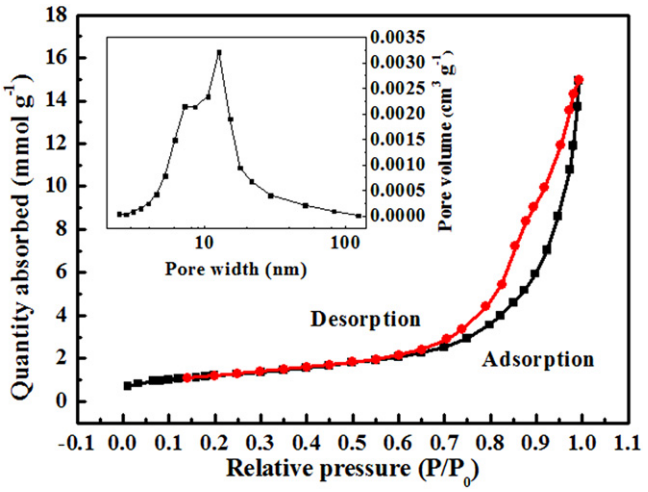

Fig. 4. Nitrogen adsorption–desorption isotherm and Barret–Joyner–Halenda (BJH) pore size distribution plot of the obtained sea urchin-like TiO_2 microspheres.

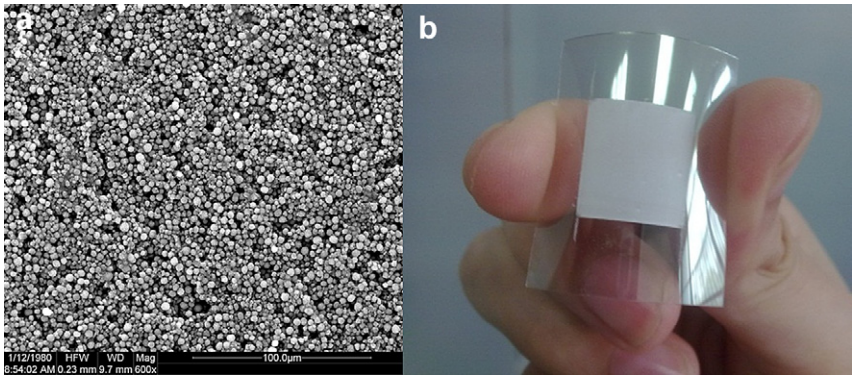

Fig. 5. SEM image of the film electrode made of sea urchin-like TiO_2 microspheres (a) and the photograph of TiO_2 microsphere-based film on ITO–PET (b).

among the TiO_2 microspheres and connection between TiO_2 film and flexible ITO–PET substrate.

As mentioned above, the hierarchical TiO_2 microspheres are composed of TiO_2 nanoparticles with diameter smaller than 20 nm. It has been reported that such small TiO_2 nanoparticles can be used as cement to enhance the particle necking in the binder-free paste [5,11–13], and plenty of such small TiO_2 nanoparticles existed between the hierarchical microspheres can play an important role as "nanoglue" to link the hierarchical microspheres [14]. During drying process of the paste at low temperature, interparticle connection can be assumed to proceed by dehydration of hydrogen-bonded network of TiO_2 nanoparticles. This hydrogen-bonded network can be effectively introduced by the addition of the TiO_2 with small diameter as cement, in which TiO_2 surfaces are covered with hydroxyl groups [11].

In our case, it is reasonable to assume the hydrogen-bonding connection of main particles can be enhanced by the large amount of the small TiO_2 particles which can produce sufficient hydroxyl groups to react with the surface of main hierarchical microspheres. Therefore, the small particles between the hierarchical TiO_2 microspheres can make a good connection with another hierarchical microsphere due to the above-mentioned necking effect. Such TiO_2 microsphere necking is favourable for flexible DSSCs due to its excellent particle interconnection, and resulting in less charge recombination and advantageous electron transfer in the film electrode. Meanwhile, it gives the binder-free paste sufficient viscosity, and resulting in an excellent adhesion to the flexible plastic substrate.

3.2. Electrochemical impedance spectrum (EIS) analyses

To investigate the electron transfer of the flexible solar cells, electrochemical impedance spectrum (EIS) was applied in our case. Fig. 6 shows the EIS spectra of the flexible DSSCs fabricated with sea urchin-like TiO_2 microspheres or P25 nanoparticles under AM 1.5 illuminations. The electron lifetime (τ_n) in the solar cell can be obtained by the position of the low frequency peak in the Bode plots through $\tau_n = 1/(2\pi f)$ (f means the frequency of superimposed ac voltage) [22]. As can be seen from the Bode plots in Fig. 6a, the f values for the hierarchical TiO_2 microsphere and the P25 film electrodes are 2.55 and 3.74 Hz, respectively. Therefore, the electron lifetimes of the hierarchical TiO_2 microsphere and the P25 nanoparticles film electrodes are calculated to be 62.4 and 42.5 ms, respectively. Obviously, the hierarchical TiO_2 microsphere electrode shows a longer electron lifetime as compared to the P25 electrode.

As can be seen from the Nyquist plots in Fig. 6b, there are two main semicircles. A simple equivalent circuit model, as exhibited in the inset of Fig. 6b, was used to simulate the solar cells. The corresponding fitted, where R_s represents the serial resistance, which is mainly influenced by the sheet resistance of the substrate and electrical contact between the conductive ITO–PET/TiO_2 interfaces, R_1 represents the impedance with charge transfer at the platinum counter electrode and/or electrical contact between TiO_2 particles, and R_2 represents the impedance related to charge transfer process at TiO_2/dye/electrolyte interfaces [4,13]. The corresponding fitted R_s, R_1 and R_2 values for the flexible solar cells are shown in Table 1. As can be seen, all the fitted resistances of the hierarchical TiO_2

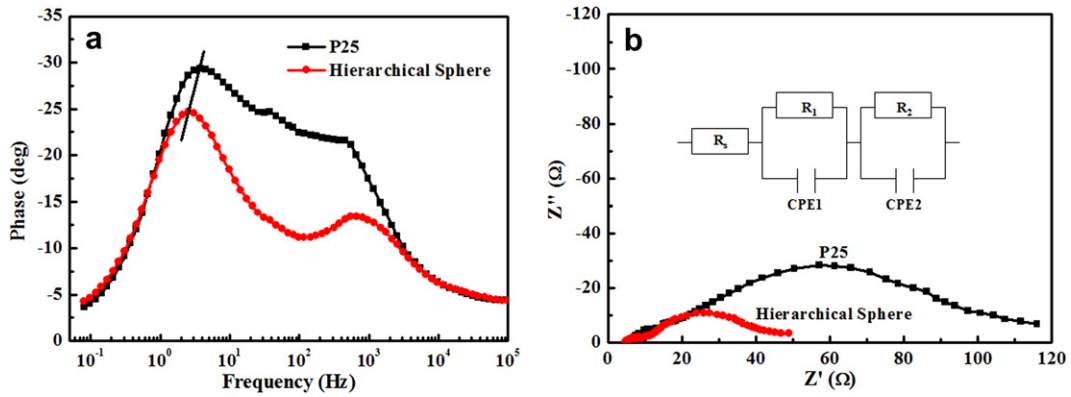

Fig. 6. Bode (a) and Nyquist (b) plots of the flexible DSSCs based on sea urchin-like TiO_2 microspheres and commercial TiO_2 (P25) nanoparticles under AM 1.5 illumination.

Table 1
The photoelectrochemical parameters of flexible solar cells fabricated with TiO_2 microsphere or P25 electrode.

Solar cell	$R_s/\Omega\ cm^2$	$R_1/\Omega\ cm^2$	$R_2/\Omega\ cm^2$	$J_{sc}/mA\ cm^{-2}$	V_{oc}/V	FF	$\eta/\%$	Dye-loading/10^{-8} mol cm^{-2}
TiO_2 microsphere-based cell	4.58	7.43	28.18	11.49	0.67	0.56	4.32	7.7
P25-based cell	5.60	18.11	101.6	6.18	0.66	0.54	2.21	4.1

microsphere-based cell are lower than those of the P25-based cell, and therefore it is easy to conclude the superiority of the hierarchical TiO_2 microspheres as compared to the P25 nanoparticles.

The smaller R_s of the hierarchical TiO_2 microsphere-based cell as compared to the P25-based one can be mainly attributed to the high adhesion of TiO_2 film to ITO–PET substrate, which derived from the cement effect of small TiO_2 nanoparticles to the hydrophobic surface of the plastic substrate as discussed above. The better electrical contact between the conductive ITO–PET/TiO_2 interfaces can lead to the decreased R_s of the hierarchical TiO_2 microsphere-based cell. Because R_1 represents the impedance with charge transfer at the platinum counter electrode and/or electrical contact between TiO_2 particles, the smaller R_1 of the hierarchical TiO_2 microsphere-based cell indicates the reduced impedance among the hierarchical TiO_2 microspheres. Due to the small nanoparticle aggregation, the present one-dimensional nanoribbons and necking effects, the boundaries between nanoparticles and hierarchical microspheres can be diminished and facilitates the electron transfer in the TiO_2 film, which leads to the declined R_1.

R_2 represents the impedance related to charge transfer process at TiO_2/dye/electrolyte interfaces. Similarly, the reduced R_2 of the hierarchical TiO_2 microsphere-based cell implies the declined resistance of electron transfer at TiO_2/dye/electrolyte interfaces. In our case, a quasi-solid-state electrolyte containing ionic liquid (DMPII) as shown in Fig. 7a was applied to the solar cell. It is obvious that this electrolyte has relatively high viscosity, which would result in poor penetration into the TiO_2 film and insufficient contact of electrolyte with the TiO_2 particles, whereas it is well realized that a full contact of electrolyte with the TiO_2 particles in the film plays an important role when applying such quasi-solid-state electrolyte with high viscosity and poor penetration into the TiO_2 film, and insufficient contact of electrolyte with the TiO_2 particles can lead to an enhanced impedance of electron transfer from electrolyte to TiO_2, thus to an enlarged R_2 in the solar cell. Because of the relatively larger diameter (~3 μm) of the hierarchical TiO_2 microsphere, lots of macropores existed among the TiO_2 microspheres as can be seen from SEM image (Fig. 7b) of TiO_2 microsphere film. These macropores with ~μm pore width are wide enough to allow the quasi-solid-state electrolyte to penetrate into TiO_2 film. However, the SEM image (Fig. 7c) of P25 film displays a very smooth surface, and the inset high magnification SEM image in Fig. 7c shows much smaller pores as compared to the TiO_2 microsphere film, which is not beneficial for the penetration of quasi-solid-state electrolyte. Moreover, the macropores are beneficial for the diffusion of the quasi-solid-state electrolyte in the hierarchical TiO_2 microsphere film, and resulting in the reduction of impedance of electron transfer from electrolyte to TiO_2, thus the decreased R_2 value of the hierarchical TiO_2 microsphere film, which is beneficial for improving the solar cell's performance.

3.3. Open-circuit photovoltage decay (OCVD) curve analyses

The interfacial recombination of electrons plays an important role for the DSSC performance, especially for the cells fabricated at low temperature. The open-circuit voltage decay (OCVD) curve can show the main information of the interfacial recombination processes between the photoinjected electrons in the TiO_2 electrode and electrolyte qualitatively. Under the present open-circuit and dark state conditions, the electron transport resistance in the TiO_2 film does not affect the OCVD measurements because there is no current flowing through the cell, and the electron lifetime (τ_n) in DSSC can change with the cell's open-circuit voltage (V_{oc}) due to the shift of semiconductor's Fermi level [23,24]. Therefore, the effects of the electron traps on the recombination reaction can be qualitatively explained by analyzing the shapes of $\tau_n \sim V_{oc}$ relation curves. The electron lifetime (τ_n) can be derived from the OCVD measurements according to the following equation.

$$\tau_n = -\frac{k_B T}{e}\left(\frac{dV_{oc}}{dt}\right)^{-1}$$

where k_B is the Boltzmann constant, T is the temperature, e is the electron charge [23].

Fig. 8a and b show the open-circuit voltage decay and corresponding τ_n–V_{oc} curves of the flexible DSSCs fabricated with sea urchin-like TiO_2 microspheres or P25 nanoparticles. As can be seen from Fig. 8a, V_{oc} value for the P25-based cell decays significantly to only 0.1 V after ~20 s in the dark state, while V_{oc} value for the hierarchical TiO_2 microsphere-based cell can still maintain at 0.4 V even after 100 s in the dark condition, indicating much lower decay

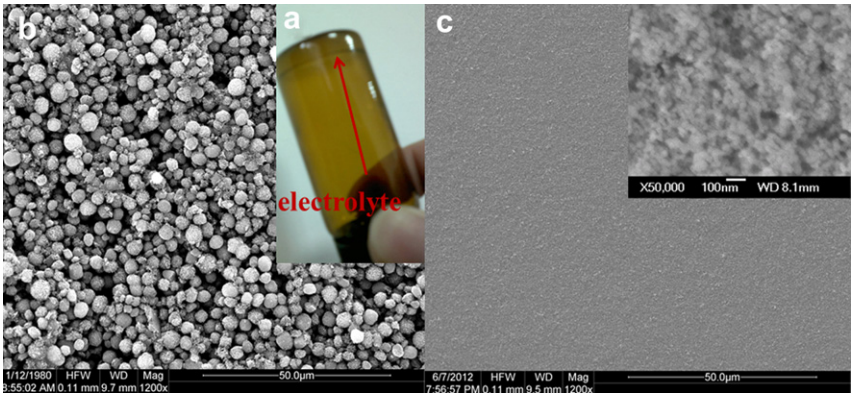

Fig. 7. Photograph of the quasi-solid-state electrolyte in brown bottle (a), SEM images of the film electrode made of sea urchin-like TiO_2 microspheres (b) and P25 (c). (For interpretation of the references to colour in this figure legend, the reader is referred to the web version of this article.)

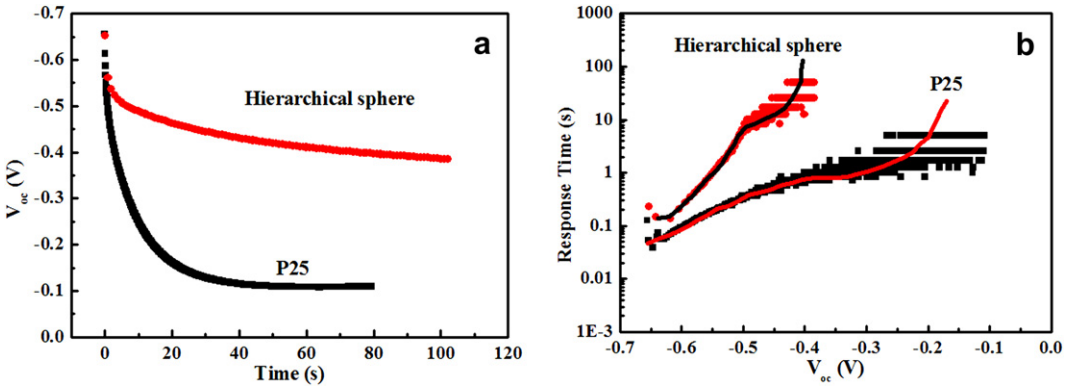

Fig. 8. Open-circuit voltage decay and τ_n–V_{oc} curves of the flexible DSSCs based on sea urchin-like TiO_2 microspheres and P25 nanoparticles.

rate, longer electron lifetime and reduced recombination as compared to the P25-based cell. The τ_n–V_{oc} relation curves can be obtained from Fig. 8a according to the above equation. As shown in Fig. 8b, the electron lifetime (τ_n) shows an exponential dependence at the V_{oc}, and the electron lifetime of the hierarchical TiO_2 microsphere-based cell is much longer than that of the P25-based cell. This phenomenon about electron lifetime can be understandable according to Bisquert and Zaban's suggestion. In their model, which could explain the shape of τ_n–V_{oc} curve qualitatively, the electron lifetime is mainly affected by the surface state traps in the TiO_2 film. Typically, three voltage-dependent regions in which the lifetime is dominated by different factors: a constant lifetime at high-voltage related to free electrons, an exponential increase at medium-voltage region due to internal trapping and detrapping, and an inverted parabola at low-voltage that corresponds to the reciprocal of the density of levels of acceptor electrolyte species [23,24]. It is obvious that the significantly increased electron lifetime can be obtained by the hierarchical TiO_2 microsphere electrode, which is ~2 or more orders of magnitude than that of the P25-based cell at middle- and low-voltage regions. Therefore, it can be concluded that the recombination stemmed from the surface trapping and detrapping is much less in the hierarchical TiO_2 microsphere electrode than in the P25 electrode. This result is in good agreement with the above observation from the Bode plots in Fig. 6a.

As discussed above, TiO_2 microsphere is constructed by hierarchical TiO_2 nanoribbons and nanoparticle-aggregated TiO_2 particles. The interconnection between TiO_2 nanoparticles can be developed well based on the aggregation and hierarchical structure. Comparing with the dispersed P25 nanoparticles, the particle boundaries can be decreased tremendously in the hierarchical microsphere electrode, resulting in less surface trapping and enhancement of the electron transfer in the film. Furthermore, the one-dimensional structure of nanoribbons can also supply direct electron pathway to facilitate the electron transfer. Additionally, the small particle necking effect as mentioned above can also strengthen the particle connection between TiO_2 microspheres further, and ensure less hurdles when electron transferred from one microsphere to another. The above factors lead to much longer electron lifetimes than that in P25 electrode, which can be reflected in τ_n–V_{oc} relation curves, especially at the middle- and low-voltage regions.

3.4. Photovoltaic performance analyses

Fig. 9 shows the photocurrent–voltage (I–V) curves of the flexible DSSCs fabricated with sea urchin-like TiO_2 microspheres and P25 nanoparticles. The values of short-circuit current (J_{sc}), open-circuit voltage (V_{oc}), fill factor (FF) and conversion efficiency (η) of the solar cells are shown in Table 1. As can be seen, all of the J_{sc}, V_{oc}, FF and η values are enhanced after replacement of P25 with the hierarchical TiO_2 microspheres. Moreover, the conversion efficiency of the hierarchical TiO_2 microsphere-based cell is almost twice as much as that of the P25-based one. As can be observed from the I–V curves and Table 1, the main factor controlling the efficiency can be ascribed to J_{sc} value since all other parameters are nearly the same. The dye-loaded amount of the TiO_2 microsphere film is much higher than that of the P25 film as shown in Table 1. The enhanced dye-loaded amount due to large surface area of the sea urchin-like TiO_2 microspheres can supply more excited photoelectrons, and resulting in the enhanced J_{sc} value. Furthermore, the special hierarchical structure of the TiO_2 microspheres should be another main factor for the much better performance as compared to the P25-base cell. As discussed in the above sections, due to the hierarchical microspheres, TiO_2 particles in the film have excellent interconnections without sacrificing the specific surface area, and the one-dimensional nanoribbons presented on the surface of the microspheres facilitate the electron transfer in the film. These merits can improve the performance of the cell based on the hierarchical microspheres, while the P25-based cell shows relatively poor performance because of insufficient interconnections between P25 particles and small surface area.

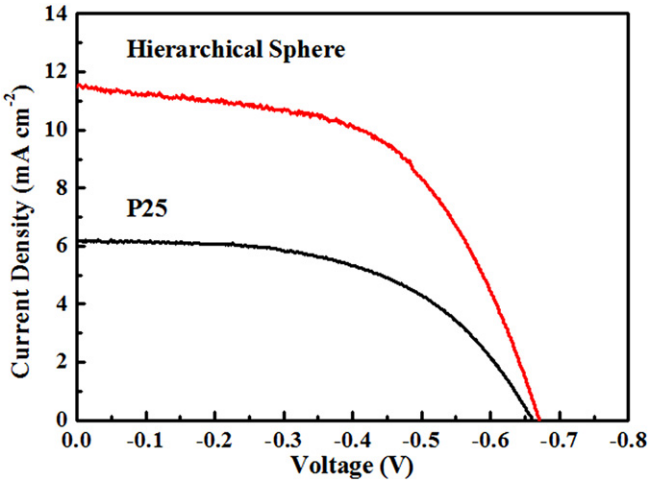

Fig. 9. Photocurrent–voltage curves of the flexible DSSCs based on sea urchin-like TiO_2 microspheres and P25 nanoparticles.

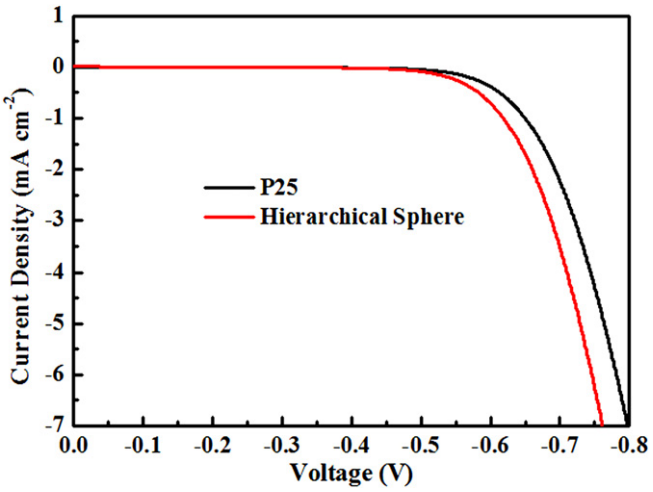

Fig. 10. Dark current–voltage curves of flexible DSSCs based on sea urchin-like TiO_2 microspheres and P25 nanoparticles.

Although electron lifetime has also major implication on the V_{oc} value of solar cell, the present TiO_2 microsphere-based cell only displays 10 mV higher than that of the P25-based one. From the dark current curves of both flexible solar cells shown in Fig. 10, it can be found that the dark current of TiO_2 microsphere-based cell is larger than that of P25-based one, which results in more V_{oc} loss as compared to the P25-based cell. This drawback can be attributed to the macropores in the present TiO_2 microsphere film. Although the macropores in the TiO_2 microsphere film is beneficial for the quasi-solid-state electrolyte contacting with TiO_2 microspheres, it may also increase the back electron transfer from substrate to electrolyte, which would result in larger dark current, consequently lower the V_{oc} of the solar cell [25]. This disadvantage made the decrease of V_{oc} of the TiO_2 microsphere electrode although it has longer electron lifetime. As a result, V_{oc} of the TiO_2 microsphere electrode was similar (just 10 mV higher) to that of P25-based electrode.

4. Conclusions

Sea urchin-like anatase TiO_2 microspheres with hierarchical structure were prepared by solvothermal method, and were applied for fabricating quasi-solid-state flexible dye-sensitized solar cells by using a simple method of mixing it with ethanol. It is found the hierarchical TiO_2 microsphere-based solar cell not only shows high specific surface area, but also enhances the particle interconnections, and resulting in lower charge recombination. In addition, the macropores in TiO_2 microsphere-based solar cell is favourable for the quasi-solid-state electrolyte penetration. Hence, the hierarchical TiO_2 microsphere-based solar cell shows an encouraging conversion efficiency of 4.32%, which is much better than that of commercial TiO_2 (P25)-based one. We anticipate that this simple preparation method by using sea urchin-like anatase TiO_2 microspheres will open up an alternative avenue for the development of flexible DSSCs.

Acknowledgements

This work was supported by the Natural Science Foundation of China (20871096, 20901061, 20973128, 21271146), the Fundamental Research Funds for the Central Universities (2081003) of China, and Key Lab of Novel Thin Film Solar Cells (KF201111).

References

[1] B. O'Regan, M. Gratzel, Nature 353 (1991) 737–739.
[2] S. Ito, M.K. Nazeeruddin, P. Liska, P. Comte, R. Charvet, P. Pechy, M. Jirousek, A. Kay, S.M. Zakeeruddin, M. Gratzel, Prog. Photovoltaics 14 (2006) 589–601.
[3] J.M. Kroon, N.J. Bakker, H.J.P. Smit, P. Liska, K.R. Thampi, P. Wang, S.M. Zakeeruddin, M. Gratzel, A. Hinsch, S. Hore, U. Wurfel, R. Sastrawan, J.R. Durrant, E. Palomares, H. Pettersson, T. Gruszecki, J. Walter, K. Skupien, G.E. Tulloch, Prog. Photovoltaics 15 (2007) 1–18.
[4] N.G. Park, K.M. Kim, M.G. Kang, K.S. Ryu, S.H. Chang, Y.J. Shin, Adv. Mater. 17 (2005) 2349–2353.
[5] X. Li, H. Lin, J.B. Li, N. Wang, C.F. Lin, L.Z. Zhang, J. Photochem. Photobiol., A 195 (2008) 247–253.
[6] T. Yamaguchi, N. Tobe, D. Matsumoto, H. Arakawa, Chem. Commun. (2007) 4767–4769.
[7] S.S. Kim, J.H. Yum, Y.E. Sung, J. Photochem. Photobiol., A 171 (2005) 269–273.
[8] H. Lindstrom, A. Holmberg, E. Magnusson, L. Malmqvist, A. Hagfeldt, J. Photochem. Photobiol., A 145 (2001) 107–112.
[9] L. Yang, L.Q. Wu, M.X. Wu, G. Xin, H. Lin, T.L. Ma, Electrochem. Commun. 12 (2010) 1000–1003.
[10] M. Durr, A. Schmid, M. Obermaier, S. Rosselli, A. Yasuda, G. Nelles, Nat. Mater. 4 (2005) 607–611.
[11] T. Miyasaka, M. Ikegami, Y. Kijitori, J. Electrochem. Soc. 154 (2007) A455–A461.
[12] T. Miyasaka, Y. Kijitori, M. Ikegami, Electrochemistry 75 (2007) 2–12.
[13] K. Fan, C. Gong, T. Peng, J. Chen, J. Xia, Nanoscale 3 (2011) 3900–3906.
[14] Y. Li, W. Lee, D.K. Lee, K. Kim, N.G. Park, M.J. Ko, Appl. Phys. Lett. 98 (2011).
[15] K. Fan, T.Y. Peng, J.N. Chen, K. Dai, J. Power Sources 196 (2011) 2939–2944.
[16] D.S. Zhang, T. Yoshida, T. Oekermann, K. Furuta, H. Minoura, Adv. Funct. Mater. 16 (2006) 1228–1234.
[17] U.N. Maiti, S. Maiti, S. Goswami, D. Sarkar, K.K. Chattopadhyay, Crystengcomm 13 (2011) 1976–1983.
[18] Y. Liu, H.M. Xu, H. Wang, W.X. Zhao, C.L. Liang, M.Y. Zhong, H. Shen, Appl. Phys. A: Mater. Sci. Process. 102 (2011) 127–130.
[19] J. Ye, W. Liu, J. Cai, S. Chen, X. Zhao, H. Zhou, L. Qi, J. Am. Chem. Soc. 133 (2010) 933–940.
[20] J. Chen, T. Peng, K. Fan, J. Xia, J. Mater. Chem. 21 (2011) 16448–16452.
[21] Z.S. Wang, H. Kawauchi, T. Kashima, H. Arakawa, Coord. Chem. Rev. 248 (2004) 1381–1389.
[22] R. Kern, R. Sastrawan, J. Ferber, R. Stangl, J. Luther, Electrochim. Acta 47 (2002) 4213–4225.
[23] J. Bisquert, A. Zaban, M. Greenshtein, I. Mora-Sero, J. Am. Chem. Soc. 126 (2004) 13550–13559.
[24] A. Zaban, M. Greenshtein, J. Bisquert, Chemphyschem 4 (2003) 859–864.
[25] P.J. Cameron, L.M. Peter, S. Hore, J. Phys. Chem. B 109 (2005) 930–936.